Electromagnetic Stir Casting Parameters and Squeeze Pressure Effects on Mechanical Properties of AA2014 alloy MMC and Hybrid MMC

Shashi Prakash Dwivedi, Satpal Sharma, Raghvendra Kumar Mishra

School of Engineering, Gautam Buddha University, Greater Noida, Gautam Buddha Nagar, U.P. 201310, India

Abstract

The main problem faced in the electromagnetic stir casting is the selection of optimum combination of input variables for achieving the required mechanical properties of composites. This problem can be solved by the development of relationship between the electromagnetic parameters and the tensile strength of composite by response surface methodology. This work focuses on the review of electromagnetic stir casting parameters effect on Mechanical Properties of MMC and Hybrid MMC. From the exhaustive review, it was observed that for better mechanical properties, lower porosity and finer grain structure of composite higher stirring current, higher stirring time and lower matrix pouring temperature required.

1. Introduction

In a variety of applications of casting, dendritic microstructure is not enviable as it results in poor mechanical properties. Enhancing the fluid flow of melted matrix alloy in the mushy zone by mechanical stirring is one of the ways to suppress this dendritic [1]. Quite a lot of manufacturing techniques have been made-up for fabrication of metal matrix composites or hybrid metal matrix composites. One of the accepted ways of generating non-dendritic microstructure is to stir the liquid metal during solidification using an electromagnetic force field [2, 3]. In metal matrix composites fabrication process, the magnetic field is applied to produce a magneto hydrodynamic effect to improve the melt flow prominent to homogenous reinforcement distribution in matrix [4]. In electromagnetic stir casting, a rotating or alternating magnetic field used to refine the grain size of the cast [5].

The theoretical approach to explain the effect of an external magnetic field on melt pool dynamic of an electromagnetic stir casting process is based on the involvement of two correlated mechanisms: First, the interaction between a magnetic field and moving and conducting fluid with velocity field will induce a current density inside the moving melt pool. Second, a temporal inhomogeneous magnetic field will induce an electric field into an electrically conducting media that will in turn induce eddy currents. Both current densities are described by Ohm's law:

$$\vec{J} = \sigma \, (\vec{E} + \vec{v} \times \vec{B}) \qquad (1)$$

With $\vec{J}$, σ, $\vec{E}$, $\vec{v}$ and $\vec{B}$ being induced current density, temperature depending electrical conductivity of the fluid, electric field, velocity field and the external magnetic flux density, respectively. Interaction between the induced current density and the external magnetic field entails a Lorentz force inside the fluid: induced current density and the external magnetic field entails a Lorentz

force inside the fluid:

$$\vec{F} = \vec{J} \times \vec{B} \qquad (2)$$

2. Literature Review

Large volume of work was earlier carried on fabrication of metal matrix composites by electromagnetic stir casting process and characterization of hybrid metal matrix composites before and after heat treatment with respect to mechanical and tribological properties. Review of Electromagnetic Stir Casting and its Process Parameters for the Metal Matrix Fabrication are given in Table 1.

3. Fabrication of metal matrix composite by EMS

Figure 2 presents the representation of electromagnetic stir casting set-up to fabricate metal matrix composite. A thermocouple is inserted in graphite crucible and it gives the feedback of the temperature of metal matrix composite during stirring. The argon gas can be used during the mixing of MMC or hybrid MMC. Coolant is used to provide the proper cooling to the windings of motor and vacuum pump is used to provide vacuum inside the box to prevent casting defects.

After the preparation of the MMC/hybrid MMC by the electromagnetic stir casting technique, the melt composites can be transferred to the universal testing machine (UTM) for squeeze pressure. The squeeze pressure is applied in mushy zone to eliminate the porosity and solidification shrinkage as shown in Figure 2.

4. Response surface methodology (RSM)

RSM is a set of mathematical and statistical methods to estimate interactions between a collection of quantitative independent variables and one or more responses. The RSM makes possible to estimate process variables that may or may not have significant outcome in the foremost response. The optimization of electromagnetic stir casting parameters is an essential step in the processing of MMCs. The electromagnetic stir casting process optimization implies the evaluation of squeeze pressure, stirring current, stirring time and pouring temperature of matrix [13].

Table 1: Electromagnetic Stir Casting and its Process Parameters

Ref. No.	Author's Name (Year)	Conclusion and Results
18	E.J. Zoqui et al. (2002)	1. The liquidus temperature of A356 was observed 609^0C. 2. Solidus temperature of A356 was found 554^0C. 3. A356 alloy was melted in an electric melting furnace. 4. The semi-solid range was 55^0 C. 5. Power-600 W, 900 W, 1200 W. 6. Frequency- 60 Hz 7. Current of 10, 13 and 15.4 A for 35, 40 and 45 V, respectively 8. Higher electromagnetic power, i.e. 1200 watt produced a very refined rheocast structure
19	S. Nafisi et al. (2006)	1. For pouring temperature of 690^0C, the grain structure is quite coarse with an average grain size of ~200 µm. 2. By reducing the pouring temperature to 660^0C, the grain size was approximately the same and no significant differences detected in the structure. 3. At 630^0C, the columnar dendritic structure changed to equiaxed morphology and the grain size has drastically reduced by almost 70%. 4. In all above process stirring time was kept constant 660 seconds
20	C.G. Kang et al. (2007)	1. Pouring temperature- 630^0C to 715^0C. 2. The 60 Hz of frequency and 220V of electric power was used with current 3. Input Current- 60 to 100 amperes. 4. Stirring time was set up as 30 s, 60 s and 90 s to compare the microstructure
21	Dehong Lu et al. (2007)	1. Poured into the graphite crucible at 750^0C 2. In the electromagnetic stirring equipment, and cooled at a constant cooling rate 8 ^0C/min. 3. As soon as the temperature of the melt reached 690^0C, the melt was stirred by the rotary magnetic field under continuous cooling conditions. 4. A series of stirring current was applied, i.e., 32, 28, 24, 20, 16, 12, 6, 4 and 0A. 5. Once the temperature of the melt reached 630^0C, electromagnetic stirring stopped. 6. The grain size structure was weakened with the decreasing of the stirring current, and vanished rapidly at current lower than 12 A.
22	C. G. Kang et al. (2008)	1. Microstructures coarsened when stirring occurred in the liquid phase at melt temperatures greater than 675°C, but were fine and globular when stirring at a melt temperature of 655°C. 2. The Stirring current also affected the microstructures by somewhat crushing the dendritic microstructures at 60 A, but the solid particles coarsened at 80 A due to the attraction and recombination of the adjacent particles.
23	Zhang Xiao-li et al. (2008)	1. Solidus and liquidus temperature are 470 and 595^0C. 2. EM-stirrer was made up of a three-phase–three-pole coil, and the power of electric supply was 25 kW and frequency was 50 Hz. When alternating current circulates through the coils, a changing electromagnetic field would be produced, and then an induced current J generates in the metal according to Faraday's law, so an electromagnetic force (Lorentz force) F would be imposed on the molten metal.
24	C. G. Kang et al. (2009)	1. When liquid segregation occurred significantly during rheoforging of Al6061 alloy, strengths as low as 268 MPa were observed. 2. Rheoforged Al6061 alloy with uniform distribution of solid and liquid phase (no segregation) within the microstructure showed good mechanical properties with tensile strengths of 341 MPa
25	T. W. Kim et al. (2009)	1. Porosity was observed at very low stirring current 2. No vortex on the free surface generated at 20–40 A of electrical stirring current. 3. Air was trapped in the center of the material with excessive vortex occurred at 60 A. 4. Pouring temperature 720^0C.
26	N. Barman et al. (2009)	1. Numerical and experimental studies on transport phenomena during solidification of an aluminum alloy in the presence of linear electromagnetic stirring are performed.
27	BAI Yue-long et al. (2009)	1. Stainless steel crucible was used, whose dimension was 160 mm in height and 80 mm in diameter and its preheat temperature was 200^0C. 2. When the pouring temperature of 670^0C is adopted, the primary α(Al) particles are dendritic with large size, but when the pouring temperature is decreased to 650^0C, most of the primary α(Al) particles are rosette-like and the particle size becomes large. If the pouring temperature continues to decrease to 630^0C, most of the primary α(Al) particles are globular with small particle size.

IJARI

| 28 | Wang Jing et al. (2010) | 1. The liquidus temperature and eutectic temperature were about 615^0C and 577^0 C, respectively.
2. The alloy was melted in a stainless steel crucible with a 104mm diameter and a length of 150mm. There was a layer of boron nitride coating on the inner surface of the crucible to prevent a reaction between the crucible and aluminium melt.
3. The frequency was set to 25 Hz and the current was 30A in these series of experiments.
4. Stainless steel crucible was preheated to about 550^0C.
5. The pouring temperature ranged between 630^0C and 690^0C for the superheat variation.
6. The cooling rate in the crucible was about 0.5^0Cs−1.
7. Globular structure is apparent at the pouring temperature of 630^0C. |
29	C. Mapelli et al. (2010)	1. Solidification thermal range: 615–655^0C. 2. This alloy has been cast in all the experimental trials at 685^0C. 3. Frequency: 15 Hz 4. Stirring current: 10-160 ampere. 5. Refinement of the grain size as the current intensity increases
30	Gab Chung et al. (2012)	1. Stirring current (A): 5, 10, 20, 30, 40, 50, and 60 2. Stirring time (s): 60, 90, 120, and 200 3. Vacuum pressure (kPa): 80, 50, 20, and 5 4. Pouring temperature: 620^0C. 5. At the pouring temperature of 620^0C , the Optimum EMS stirring current and time were obtained 30 A and 60 s, respectively. The vacuum level with the least presence of the porosity was determined at 50 kPa, while further increase in the vacuum level (decrease in the applied pressure) resulted in increase in the presence of the porosity.
31	Prabhkiran Kaur et al. (2012)	1. Stirring of the melt was carried out for 2 min in the mushy zone under a temperature range from 625°C to 645°C in a graphite crucible which was preheated to 300°C. 2. The current was increased gradually from 0 to 30 A in orders to increase the stirring speed of the material. 3. Pouring temperature: 620°C±5°C
32	Y.D. Yu et al. (2013)	1. The melt was poured into a preheated (to 350^0C) stainless steel mold with a diameter of 45 mm, height of 200 mm and a wall-thickness of 10 mm. 2. Without magnetic field UTS-232 MPa, with magnetic field UTS- 254 MPa.
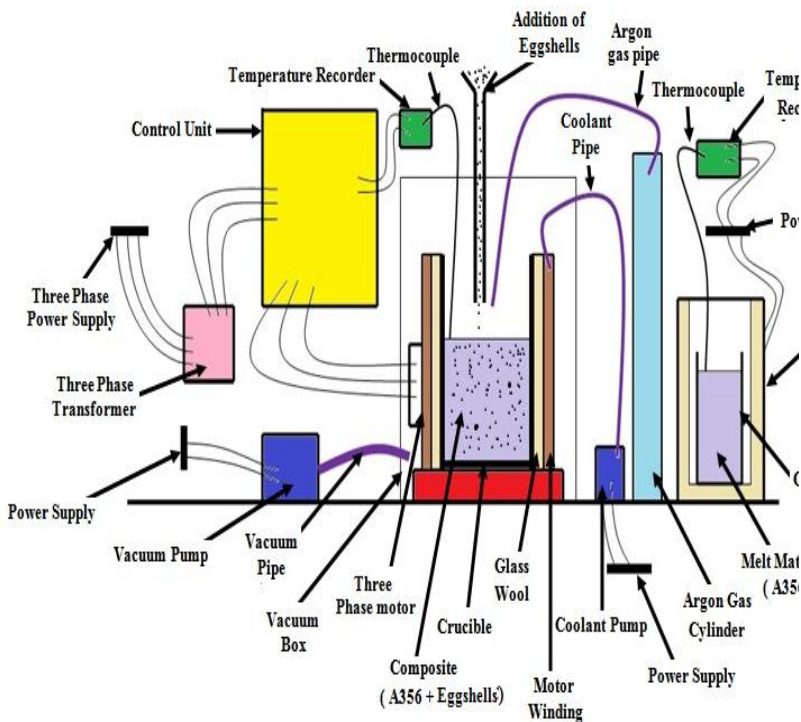
Fig. 1: Experimental Set-up of Electromagnetic Stir Casting Process
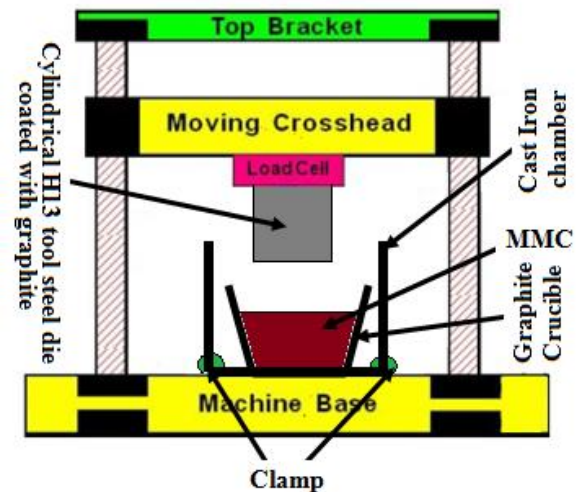

Fig. 2: Schematic diagram of squeeze casting process on UTM

The central composite design (CCD) was used to build a second order experimental model. CCD is composed of factorial points, a set of central points, and axial points equidistant to the center point. The factorial points are component of CCD of the class 2^k factorial, where k represents the number of appropriate factors or variables. The central point component in the CCD is the average of the high and low values determined in the factorial points. The central point or zero point may be defined as the region where the optimal conditions are supposed to meet. Steps

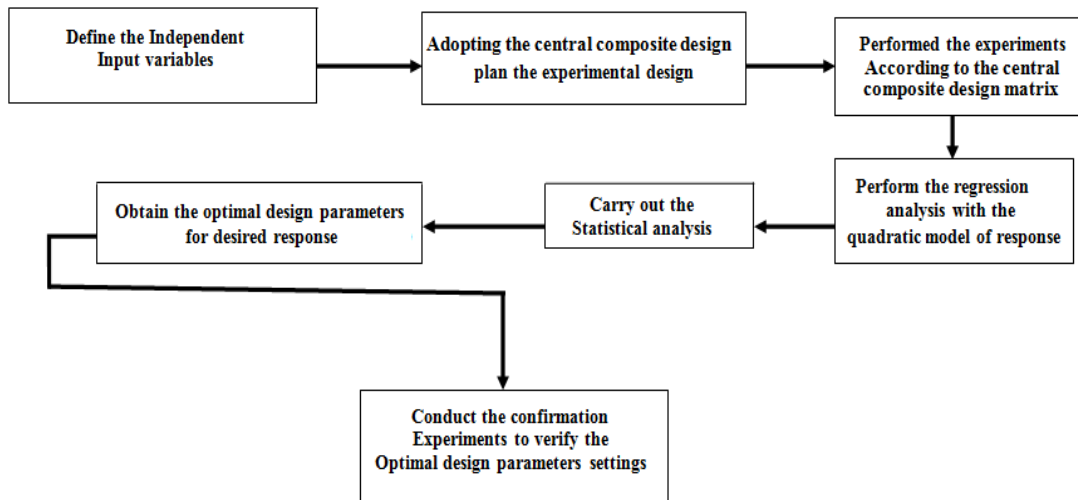involved in central composite design are given in Figure 4 [14, 15].

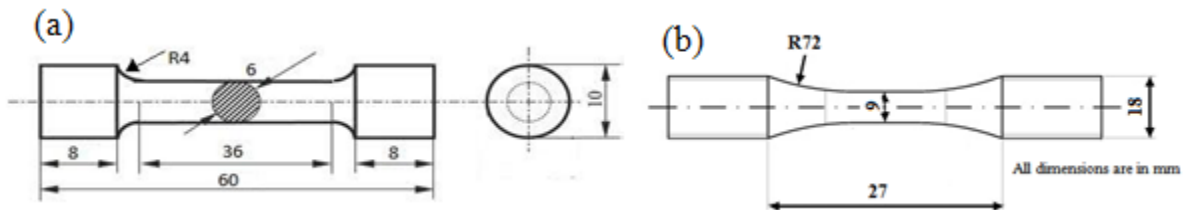**Fig. 3**: Steps involved in central composite design [20]

Fig.4: Sample specification; (a) tensile sample, (b) Fatigue sample [18]

5. Sample Preparation:

The developed composites at optimum parameters can be characterized in terms of tensile strength, fatigue strength, hardness (10 mm x 10 mm x 25 mm) and toughness (10 mm x 10 mm x 55 mm with 45^0 V notch at center of 2 mm depth). The sample sizes for tensile strength and fatigue strength are shown in Figure 3 (a & b).

6. Conclusions

The following conclusions can be drawn from the exhaustive review:-

1. Electromagnetic stir casting process followed by squeeze pressure can be adapted favorably for the fabrication of MMC and hybrid MMC.
2. Pouring temperature of matrix in crucible after melting in furnace was kept low (near to its liquidus temperature).
3. For high pouring temperature, the grain structure is quite coarse while at low pouring temperature, the columnar dendritic structure changed to equiaxed morphology and the grain size has drastically reduced.
4. Higher electromagnetic power produced a very refined structure of matrix.
5. The grain size structure was weakened with the decreasing of the stirring current, and vanished rapidly at very low current.
6. Porosity was observed at very low stirring current.
7. At very higher current excessive vortex occurred, resulting air was trapped in the centre of the material.
8. The current was increased gradually in orders to increase the stirring speed of material.
9. Higher stirring current, higher stirring time and lower matrix pouring temperature provides better mechanical properties and lower porosity.

References

[1.] Barman, N., Kumar, P., & Dutta P. (2009). Studies on transport phenomena during solidification of an aluminum alloy in the presence of linear electromagnetic stirring. Journal of Materials Processing Technology, 209, 5912–5923.

[2.] Kang C. G. & Lee S. M. (2008). Development of a new rheology forming process with a vertical-type sleeve with electromagnetic stirring. Int J Adv Manuf Technol, 39, 462–473.

[3.] Jing, W., Peijie, L., Guangbao, M., & Yuexian Z. (2010). Microstructural evolution caused by electromagnetic stirring in superheated AlSi7Mg alloys. Journal of Materials Processing Technology, 210, 1652–1659.

[4.] Yue-long, B., Jun, X., Zhi-feng, Z., & Li-kai S. (2009). Preparation of semi-solid slurry at power frequency by annulus electromagnetic stirring method. Trans. Nonferrous Met. Soc. China, 19, s531-s536.

[5.] Yu, Y.D. & Li C.X. (2013). The effect of alternative low frequency electromagnetic field on the solidification microstructure and mechanical properties of ZK60 alloys. Materials and Design, 44, 17–22.

[6.] Hassan, S.B. & Aigbodion V.S. (2013). Effects of eggshell on the microstructures and properties of Al–Cu–Mg/eggshell   particulate   composites.

http://dx.doi.org/10.1016/j.jksues.2013.03.001

[7.]   Yew, M.C., Ramli Sulong, N.H., Yew, M.K., Amalina, M.A., & Johan M.R. (2013). The formulation and study of the thermal stability and mechanicalproperties of an acrylic coating using chicken eggshell as a novelbio-filler. Progress in Organic Coatings, 76, 1549– 1555.

[8.]   Casari, D., Merlin, M., & Garagnani, G. L. (2013). A comparative study on the effects of three commercial Ti–B-based grain refiners on the impact properties of A356 cast aluminium alloy. Journal of Materials Science, 48, 4365-4377.

[9.]   Gao, L., Harada, Y., & Kumai, S. (2012). Analysis of microstructure evolution and precise solid fraction evaluation of A356 aluminum alloy during partial re-melting by a color etching method. Journal of Materials Science, 47, 6553-6564.

[10.]   Itskos, G., Rohatgi, P. K., Moutsatsou, A., DeFouw, J. D., Koukouzas, N., Vasilatos, C., & Schultz B. F. (2012). Synthesis of A356 Al–high-Ca fly ash composites by pressure infiltration technique and their characterization. Journal of Materials Science, 47, 4042-4052.

[11.]   Wang, F., Meng, X., Ma, N., Xu, J., Li, X., & Wang H. (2012). The relationship between TiB_2 volume fraction and fatigue crack growth behavior in the in situ TiB_2/A356 composites. Journal of Materials Science, 47, 3361-3366.

[12.]   Lunge, S., Thakre, D., Kamble, S., Labhsetwar, N., & Rayalu S. (2012). Alumina supported carbon composite material with exceptionally high defluoridation property from eggshell waste. Journal of Hazardous Materials, 237– 238, 161– 169.

[13.]   Gning, P. B., Liang, S., Guillaumat, L., & Pui, W. J. (2011). Influence of process and test parameters on the mechanical properties of flax/epoxy composites using response surface methodology. Journal of Materials Science, 46, 6801-6811.

[14.]   Agarwal, P., Mishra, P. K., & Srivastava P. (2012). Statistical optimization of the electrospinning process for chitosan/polylactide nanofabrication using response surface methodology. Journal of Materials Science, 47, 4262-4269.

[15.]   Dwivedi, S. P., Kumar, S., & Kumar A. (2012). Effect of turning parameters on surface roughness of A356/5% SiC composite produced by electromagnetic stir casting. Journal of Mechanical Science and Technology, 26, 3973-3979.

[16.]   Dwivedi S. P. (2014). Effect of process parameters on tensile strength of friction stir welding A356/C355 aluminium alloys joint. Journal of Mechanical Science and Technology, 28, 285-291.

[17.]   Dwivedi, S. P., Sharma, S. (2014). Effect of Process Parameters on Tensile Strength of 1018 Mild Steel Joints Fabricated by Microwave Welding. Metallography, Microstructure, and Analysis, 3, 58-69.

[18.]   E.J. Zoquia, M. Paes, E. Es-Sadiqi, "Macro- and microstructure analysis of SSM A356 produced by electromagnetic stirring," Journal of Materials Processing Technology, 120 (2002) 365–373.

[19.] S. Nafisi, D. Emadi, M.T. Shehata, R. Ghomashchi, "Effects of electromagnetic stirring and superheat on the microstructural characteristics of Al–Si–Fe alloy," Materials Science and Engineering A, 432 (2006) 71–83.

[20.]   C.G. Kang, J.W. Bae, B.M. Kim, "The grain size control of A356 aluminum alloy by horizontal electromagnetic stirring for rheology forging," Journal of Materials Processing Technology, 187–188 (2007) 344–348.

[21.]   Dehong Lu, Yehua Jiang, Guisheng Guan, Rongfeng Zhou, Zhenhua Li, Rong Zhou, "Refinement of primary Si in hypereutectic Al–Si alloy by electromagnetic stirring," Journal of Materials Processing Technology, 189 (2007) 13–18.

[22.]   C. G. Kang, S. M. Lee, "Development of a new rheology forming process with a vertical-type sleeve with electromagnetic stirring," Int J Adv Manuf Technol, 39 (2008) 462–473.

[23.]   Zhang Xiao-li, Li Ting-ju, Teng Hai-tao, Xie Shui-sheng, Jin Jun-ze, "Semisolid processing AZ91 magnesium alloy by electromagnetic stirring after near-liquidus isothermal heat treatment," Materials Science and Engineering A, 475 (2008) 194–201.

[24.]   C. G. Kang, S. M. Lee, "The effect of solid fraction and indirect forging pressure on mechanical properties of wrought aluminum alloy fabricated by electromagnetic stirring" Int J Adv Manuf Technol, 42 (2009) 73–82.

[25.]   T. W. Kim, S. M. Lee, C. G. Kang, B. M. Kim, "Rheological forging process of A6061 wrought aluminum alloy with controlled liquid fraction by electromagnetic stirring system" Int J Adv Manuf Technol, 40 (2009) 242–252.

[26.]   N. Barman, P. Kumar, P. Dutta, "Studies on transport phenomena during solidification of an aluminum alloy in the presence of linear electromagnetic stirring," Journal of Materials Processing Technology 209 (2009) 5912–5923.

[27.]   Bai Yue-long, Xu Jun, Zhang Zhi-feng, Shi Li-kai, "Annulus electromagnetic stirring for preparing semisolid A357 aluminum alloy slurry," Trans. Nonferrous Met. Soc. China 19(2009) 1104-1109.

[28.]   Wang Jing, Li Peijie, Mi Guangbao, Zhong Yuexian, "Microstructural evolution caused by electromagnetic stirring in superheated AlSi7Mg alloys," Journal of Materials Processing Technology, 210 (2010) 1652–1659.

[29.]   C. Mapelli, A. Gruttadauria, M. Peroni, "Application of electromagnetic stirring for the homogenization of aluminium billet cast in a semi-continuous machine," Journal of Materials Processing Technology, 210 (2010) 306–314.

[30.]   Il-Gab Chung, Amir Bolouri, Chung-gil Kang, "A study on semisolid processing of A356 aluminum alloy through vacuum-assisted electromagnetic stirring," Int J Adv Manuf Technol, 58 (2012) 237–245.

[31.]   Prabhkiran Kaur, D. K. Dwivedi, P. M. Pathak, "Effects of electromagnetic stirring and rare earth compounds on the microstructure and mechanical properties of hypereutectic Al–Si alloys" Int J Adv Manuf Technol, 63 (2012) 415–420.

[32.]   Y.D. Yu, C.X. Li, "The effect of alternative low frequency electromagnetic field on the solidification microstructure and mechanical properties of ZK60 alloys," Materials and Design, 44 (2013) 17–22.